镁/钢异种金属 CMT 对接熔钎焊连接机理

曹 睿[1]， 朱海霞[1]， 王 清[2]， 董 闯[2]， 林巧力[1]， 陈剑虹[1]
(1. 兰州理工大学 有色金属先进加工与再利用省部共建国家重点实验室，兰州 730050;
2. 大连理工大学 三束材料改性教育部重点实验室，大连 116024)

摘 要：文中用 AZ61 镁焊丝以及冷金属过渡焊接方法对接形式连接镁合金 AZ31 和镀锌钢板，在焊接过程中保持焊接速度不变，通过调节送丝速度和对钢板开不同的坡口研究不同焊接工艺参数下焊缝的表面成形、接头的力学性能和微观组织结构. 结果表明，通过调节合适的焊接参数以及坡口形式，镁-钢之间能形成焊缝成形美观、接头最大抗拉载荷达到 4.02 kN 的镁钢对接熔钎焊接头. 并且熔钎焊接头包括镁侧的熔焊接头和钢侧的钎焊接头，钎焊接头由两部分组成，一部分是坡口面上的镁与裸钢板之间的钎焊接头，另一部分是镀锌钢板上表面的镁-镀锌钢之间的钎焊接头. 镁-镀锌钢侧的钎焊连接主要由靠近镁侧的(α - Mg + MgZn) 的共晶相，以及靠近钢侧的 Fe-Al 相反应层实现连接. 无镀锌层的钢和镁连接主要依靠焊丝中的微量 Al 元素扩散到钢表面形成 Fe/Al 相来实现连接.

关键词：镁合金 AZ31；镀锌钢；冷金属过渡；熔钎焊
中图分类号：TG 456.9 **文献标识码**：A **文章编号**：0253 - 360X(2016)05 - 0037 - 04

0 序 言

近年来考虑到车辆减重、节约能源以及满足不同的服役环境等方面，异种金属连接特别是铝-钢、镁-钢的连接显得至关重要[1]. 由于 Mg-Fe 之间既没有固溶度也没有金属间化合物，因此直接连接其焊接性较差. 同时由于其熔沸点相差较大，因此目前的大量研究主要集中于镁钢的熔钎焊研究. 大量研究学者已经通过各种焊接方法例如激光焊接、电弧焊、搅拌摩擦焊以及电阻焊等方法连接这两种金属[2-6]，结果发现要实现这两种金属的连接，焊丝中的其它元素 Al，Zn 以及钢板表面的镀层或者其它的夹层都是非常关键的. 同时大量的研究也主要集中于搭接焊以及点焊等形式，而在实际应用中因对接接头具有受力状况较好、应力集中小、节约材料等特点，在工程机械中应用广泛. 因此，文中主要研究镁/钢异种金属冷金属过渡对接焊连接机理.

1 试验方法

采用 3 mm 厚的 AZ31B 镁合金板和 Q235 钢板对接焊. 焊接时因为镁板容易熔化故无需开坡口，对镀锌钢板开 30°和 60°的坡口. 采用焊丝正对坡口斜面中心部位，焊接规范如表 1 所示，焊接装置示意图如图 1 所示. 60°坡口的接头为接头Ⅰ，30°坡口的接头为接头Ⅱ. 焊接时均使用 AZ61 镁焊丝为填充金属，焊接速度为 5 mm/s 不变，保护气体是气流量为 15 L/min 的高纯氩气. 通过改变坡口角度、送丝速度即热输入和填充金属量来研究镁/钢对接焊接头的宏观形貌、微观组织、力学性能. 采用 CMT 对接焊时，当送丝速度大于 12.5 m/min 时，因焊接时电流、电压以及填充金属量过大，镁合金及镁焊丝产生严重的飞溅和烧损，不能成形. 故采用如表 1 所示的焊接工艺参数对接焊镁/钢板.

表 1 镁/钢对接焊焊接工艺参数

Table 1 Welding parameters of Mg-steel butt welded joints

试样编号	送丝速度 v_f/(m·min^{-1})	焊接速度 v/(mm·s^{-1})	焊接电流 I/A	焊接电压 U/V
02	12.5	5	158	12.8
03	12.0	5	152	12.5
04	11.5	5	140	11.5
05	11.0	5	139	10.9
06	10.5	5	130	10.9
07	10.0	5	125	10.8
08	9.5	5	115	10.6
09	9.0	5	110	10.4
10	8.5	5	108	10.2
11	8.0	5	98	9.7
12	7.5	5	93	9.6

收稿日期：2015 - 11 - 07
基金项目：973 计划前期研究专项(2014CB660810)，国家自然科学基金资助项目(51265028)及大连理工大学三束材料改性教育部重点实验室开放基金资助资目(LABKF1402)

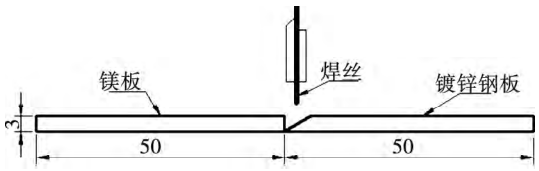

图 1 镁/钢对接焊接装置图(mm)

Fig. 1 Schematic of Mg-Steel butt welded device

2 试验结果及分析

2.1 焊接接头的宏观形貌

图 2 为送丝速度为 9 m/min 时镁/钢对接焊焊接接头的宏观形貌,从焊缝形貌可以看出,使用 CMT 对接焊镁/钢后的焊缝成形良好,焊缝表面未观察到裂纹、孔洞等焊接缺陷.

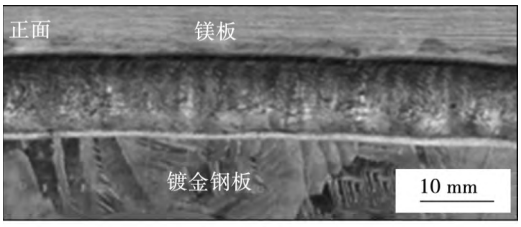

(a) 正面成形

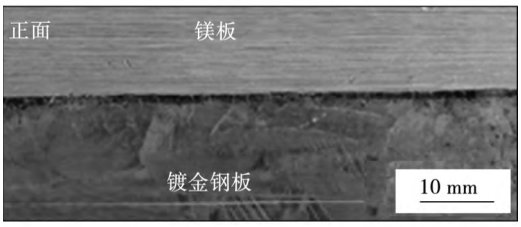

(b) 背面成形

图 2 送丝速度为 9 m/min 时镁/钢对接焊接头的宏观形貌

Fig. 2 Macro-feature of Mg-steel butt welded joint at 9 m/min of wire feed speed

图 3 为送丝速度和镁/钢对接焊焊缝熔宽的关系,由图 3 可知,随着送丝速度的增加接头 Ⅰ 和 Ⅱ 的焊缝熔宽均增加. 因为随着送丝速度的增加填充金属量增加且镁板的熔化量增加故焊缝熔宽增加.

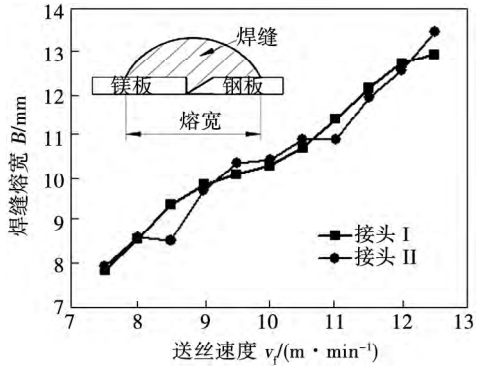

图 3 送丝速度和镁/钢对接焊焊缝熔宽的关系

Fig. 3 Relationship between wire feed speed and weld width

2.2 焊接接头的微观组织

镁/钢对接熔钎焊接头宏观组织形貌如图 4 所示. 可知镁焊丝在镁合金上的铺展润湿性比较差,对接接头具有典型的熔钎焊特征,和镁板一侧形成熔焊接头,熔焊接头的形貌是典型的镁焊接接头的形貌,在此不详细描述,见文献[7]. 而在坡口界面以及镀锌钢板表面上均形成钎焊接头,这两个钎焊接头不同,镀锌钢板表面上形成的是镁和镀锌钢板的钎焊界面 A,B 和坡口面上形成的是镁和裸钢板的钎焊连接接头 C. 其中接头连接和失效的关键部位在于钎焊界面处. 因此文中对钎焊界面处进行重点分析.

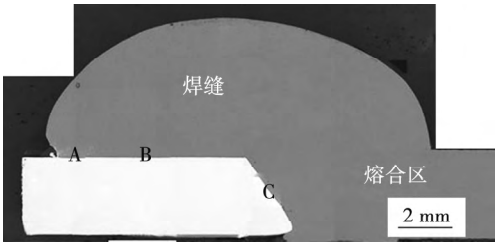

图 4 镁/钢对接焊接头横截面宏观形貌

Fig. 4 Cross-section of Mg-steel butt welded joint

图 5 为图 4 中钎焊界面 A 区焊趾处的微观组织形貌. 图 5a 为富锌区的全貌. 对富锌区组织放大如图 5b 所示,对不同的相进行能谱分析,可以发现该富锌区由($Zn + Mg_2Zn_{11}$),$MgZn_2$,MgZn 以及共晶组织($\alpha - Mg + MgZn$)相组成.

图 4 钎焊界面 B 区的组织形貌如图 6 所示,在焊缝金属和钢之间有一层分布不均匀的层片状反应层,大约 2 ~ 8 μm. 沿着图 6 箭头 EF 所示的方向进行线分析结果如图 6b 所示,同样发现在反应层从钢基体侧起依次有 Al 和 Zn 元素的富集. 根据界面处的点分析结果可知该反应层是靠近镁侧的($\alpha - Mg + MgZn$)的共晶相,以及靠近钢侧的 Fe-Al 相反应层.

钎焊界面 C 区组织形貌如图 7 所示,对 3 mm 的镀锌钢板开坡口后坡口处表面无锌,该处实现的就是镁/裸钢板钎焊连接. 沿着图 7a 箭头 GH 所示的方向进行线分析,分析结果如图 7b 所示. 对 3 mm 的镀锌钢板开坡口后坡口处表面无锌,该处的组织和镁/裸钢板钎焊界面处相似. 对该界面处进行面分析结果如图 8 所示,可知界面附近区域都不存在 Zn 元素的富集,然而 Al 元素富集在钎焊界面处,形成 Fe-Al 相的反应层. 可以看出在坡口与焊缝金属

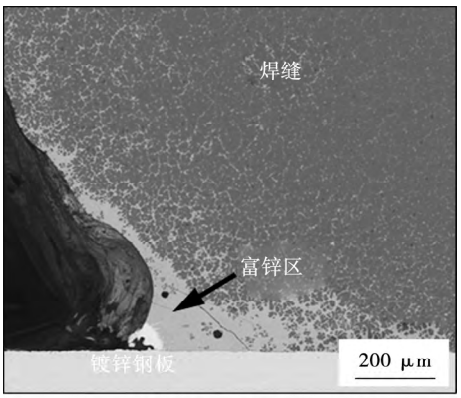

(a) 焊趾处富锌区微观组织形貌

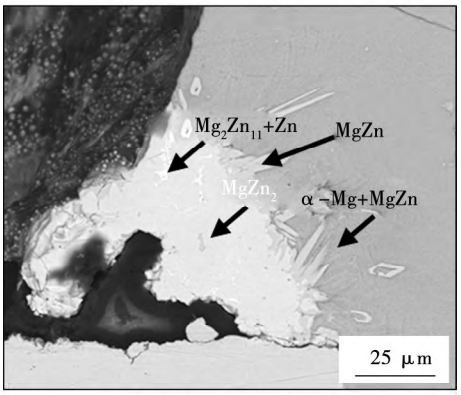

(b) 富锌区微观组织放大

图 5　图 4 中钎焊界面焊趾处 A 区富锌区组织形貌

Fig. 5　Microstructure of rich-zinc zone A at weld toe of brazed interface in Fig. 4

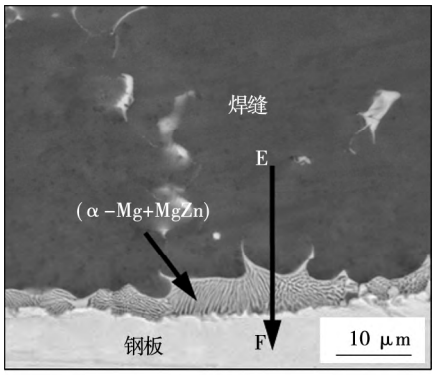

(a) 钎焊界面处B区组织形貌

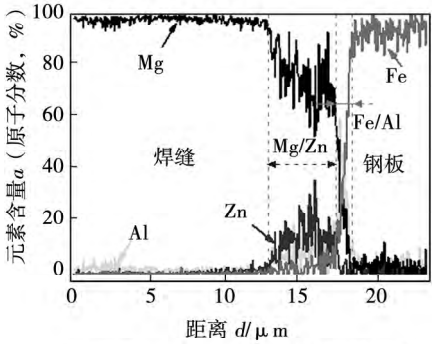

(b)沿图6a黑箭头线EF的线扫描结果

图 6　图 4 中钎焊界面处 B 区组织及线扫描结果

Fig. 6　Microstructure of brazed zone B in Fig. 4 and line scanning results

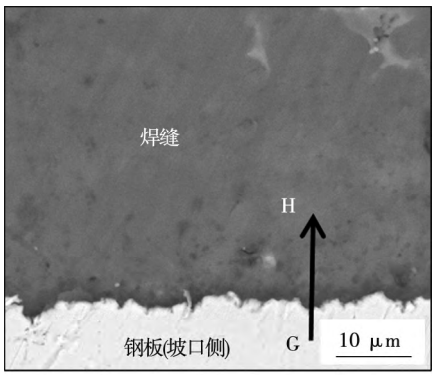

(a) 钎焊界面处C区组织

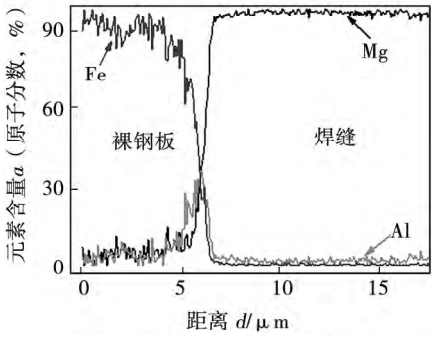

(b)沿图7a黑箭头线GH的线扫描结果

图 7　图 4 中钎焊界面处 C 区组织及线扫描结果

Fig. 7　Microstructure of brazed zone C in Fig. 4 and line scanning results

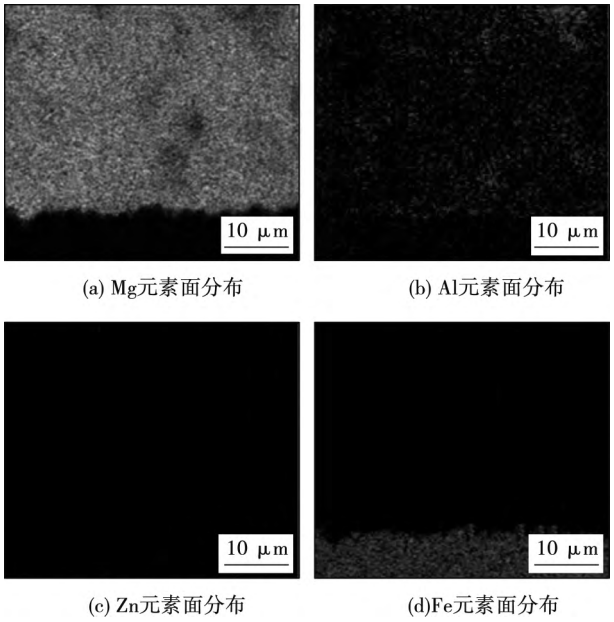

(a) Mg元素面分布　(b) Al元素面分布

(c) Zn元素面分布　(d)Fe元素面分布

图 8　图 7a 中钎焊界面处 C 区各个元素的面分布

Fig. 8　Area scanning distribution of all elements in brazed interface C in Fig. 7a

钎接处没有 Zn 元素,但在焊缝金属和钢基体之间却富集了 Al 元素,这主要是由于 Fe 元素和 Al 元素之间的亲和能力较大,从而在界面附近的液态钎料中的 Al 原子在凝固的过程中不断向含有铁溶质的界

面附近聚集,造成了 Al 元素在界面的偏聚. 从而在界面处形成 Fe/Al 相. 可以看出在无镀锌层的钢和镁焊丝形成的焊缝金属连接时,主要依靠焊丝中的微量 Al 元素扩散到钢表面形成 Fe/Al 相来实现镁/钢之间的连接.

2.3 焊接接头的力学性能

图 9 为镁/镀锌钢板 CMT 对接焊接头在不同送丝速度下的力学性能. 从图 9 可以看出当送丝速度小于 11 m/min 时,接头Ⅰ和Ⅱ的性能均是随着送丝速度增加变化不大,最大抗拉载荷大约为 2.2 kN. 而当送丝速度大于 11 m/min 时,接头Ⅰ和接头Ⅱ的性能均随着送丝速度的增加而增大,在拉伸载荷下接头Ⅰ和接头Ⅱ均断裂在钎焊界面处,断裂示意图如图 10 所示. 根据文献[8]可知在镁和镀锌钢板结合的钎焊界面 B 处界面处 Mg/Zn 共晶组织和焊缝之间的结合比较牢固,Fe/Al 相和钢基体之间的结合也比较牢固,但是 Mg/Zn 共晶相组织与 Fe/Al 相之间的结合并不好,导致在拉伸过程中 Mg/Zn 共晶相组织与 Fe/Al 相之间开裂. 这是由于,Mg/Zn 共晶相是复杂六方结构,而 Fe/Al 相是立方结构,二者相界面处的晶格错配度大且互不能溶解. 故在如图 10 所示的拉伸试验中易成为接头的薄弱区. 根据文献[8]和图 7,图 8 可知镁/裸钢板钎焊界面断裂处的连接主要靠很薄的一层 FeAl 金属间化合物和一些 Al,Mg 元素的扩散导致连接,因此在断口特征上并不能明显判断出断裂于细微的“FeAl 金属间在合物层或者一些 Al,Mg 元素的扩散层”.

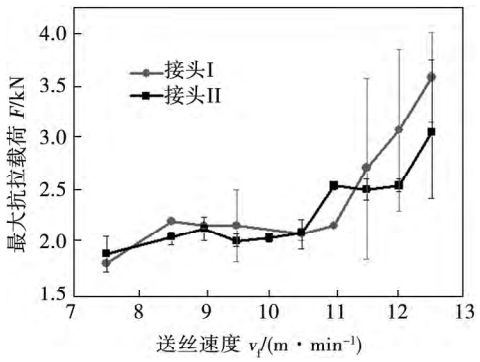

图 9 镁/钢 CMT 对接焊接头的抗拉载荷与送丝速度之间的关系

Fig. 9 Relationships between wire feed speeds and tensile load of Mg/steel butt welded joints

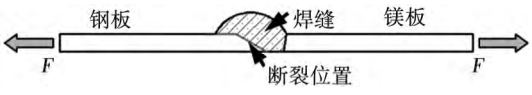

图 10 镁/钢对接焊接头断裂示意图

Fig. 10 Schematic of fracture path of Mg/steel butt welded joints

3 结 论

(1) 采用 AZ61 镁焊丝作为填充材料,使用冷金属过渡技术可以实现 3 mm 厚镁板(AZ31B)和 3 mm 厚的钢板(Q235)的对接焊接,能获得成形较美观的焊缝.

(2) 镁/钢异种金属对接焊接头是典型熔钎焊接头. 焊缝金属和镀锌钢板表面的钎焊界面生成(α-Mg + MgZn)共晶相反应层和 Fe/Al 相反应层,而焊缝金属和钢板坡口之间的钎焊界面是通过 Fe/Al相连接.

(3) 3 mm 镁板(AZ31B)和 3 mm 的钢板(Q235)的对接焊接时,焊接接头的钎焊界面处结合较熔合区和焊缝脆弱,断裂均发生在钎焊界面处. 钢板开 60° 坡口时坡口面积增加焊接接头的强度也随之增加. 焊接接头的最大抗拉载荷可以达到 4.02 kN.

参考文献:

[1] 孙景林,郭 静. 镁合金在汽车轻量化方面的应用[J]. 轻金属,2008,7:58-60.
Sun Jinglin, Guo Jing. Application of magnesium alloy to popularization of lightweight automobiles[J]. Lightweight Alloys, 2008, 7: 58-60.

[2] Chen Y C, Nakata K. Effect of surface states of steel on microstructure and mechanical properties of lap joints of magnesium alloy and steel by friction stir welding[J]. Science and Technology of Welding and Joining, 2010, 5(4): 293-298.

[3] Liu L, Qi X. Strengthening effect of nickel and copper interlayers on hybrid laser-TIG welded joints between magnesium alloy and mild steel[J]. Materials Design, 2010, 31(8): 3960-3963.

[4] Liu L, Xiao L, Feng J C, *et al*. The mechanisms of resistance spot welding of magnesium to steel[J]. Metallurgical and Materials Transactions A, 2010(41): 2651-2661.

[5] Waled M. Elthalabawy, Tahir I Khan. Microstructural development of diffusion brazed austenitic stainless steel to magnesium alloy using a nickel interlayer[J]. Materials Characterization, 2010, 61: 703-712.

[6] Li Liqun, Tan Caiwang, Chen Yanbin, *et al*. Influence of Zn coating on Interfacial reactions and mechanical properties during laser welding-brazing of Mg to steel[J]. Metallurgical And Materials Transcations A, 2012, 12(43A): 4740-4754.

[7] 曹 睿,余建永,陈剑虹,等. 镁/镀锌钢板 CMT 熔钎焊连接机制分析[J]. 焊接学报,2013,34(9): 21-34.
Cao Rui, Yu Jianyong, Chen Jianhong, *et al*. Bonding mechanism of CMT fusion-brazed joints between magnesium and galvanized steel[J]. Transactions of the China Welding Institution, 2013, 34(9): 21-34.

[8] Cao R, Zhu H X, Wang Q, *et al*. Effects of zinc coating on magnesium alloy-steel joints produced by cold metal transfer method[J]. Materials Science and Technology, 2016, 1-13. DOI: 10.1080/02670836. 2016. 1148107.

作者简介: 曹 睿,女,1977 年出生,博士,教授,博士研究生导师. 主要从事新材料的焊接性及材料的变形断裂行为. 发表论文 90 余篇. Email: caorui@lut.cn

Abstract: Residual stress after seal welding and stress by internal pressure in vacuum environment of T/R box are analyzed using finite element analysis software MSC. Marc. Optimum design method is provided afterward. Effects of shape of box, length of sides and thickness of cover plate on stress by internal pressure are investigated. Effect of stress by internal pressure on welding residual stress is analyzed as well. Reliability and the limit size of the T/R box are discussed afterward. Results shown that stress by internal pressure increases by the increasing of short length and the decreasing of thickness of cover plate. The change of long length has almost no effect on stress by internal pressure.

Key words: finite element analysis; seal welding; stress; optimum design

Numerical simulation of welding residual stress and deformation induced by electro slag welding SUN Jiamin[1], ZHU Jiayong[2], XIA Linying[2], DENG Dean[1] (1. School of Material Science and Engineering, Chongqing University, Chongqing 400044, China; 2. Construction Steel Structure Company, Shenzhen 518040, China). pp 23-27

Abstract: In order to study the feature of welding residual stress distribution and distortion induced by electro slag welding (ESW), a computational approach was developed to predict welding temperature field, welding residual stress and distortion using MSC. Marc software. In the proposed approach, a new heat source named full ellipsoid volumetric heat source with uniform density was developed to model heat input produced by ESW. The "birth and death" element technique was used to simulate the formation of weld bead. The welding residual stress distribution and deformation in the box column plate and diaphragm were calculated. Meanwhile, the transverse shrinkage and angular distortion were measured by experiment. The results show that the numerical results are in a good agreement with the measured data, and the effectiveness of the computational approach was verified. In addition, the general features of welding residual stress distribution in the ESW joint was numerically investigated.

Key words: electro slag welding; heat source with uniform density; welding residual stress; welding distortion

Dissimilar fiction stir welding of titanium alloy and aluminum alloy employing a modified butt joint configuration ZHANG Zhenhua[1], SHEN Yifu[1], FENG Xiaomei[1], LI Bo[1], HU Weiye[2] (1. College of Materials Science and Technology, Nanjing University of Aeronautics and Astronautics, Nanjing 210016, China; 2. Technology Research Institute of Nanjing Chenguang Group Co., Ltd (NCGC), China Aerospace Science and Industry Corporation (CASTC), Nanjing 210006, China). pp 28-32

Abstract: The present research employed a modified butt joint configuration into the FSW of TC4 titanium alloy and 5A06 aluminum alloy with an excess pin offset setup towards titanium alloy butt side, aiming to reduce the tool shoulder attrition, avoid butt root flaws, and study the effects of the process variables on the weld interfaces and tensile properties. Under the best FSW process condition, the examinations and analyses of macro/micro-structures, mechanical tensile properties of the dissimilar joints were conducted. The experiment results show that the joint mechanical tensile strength can reach 88.3 % of the parent aluminum alloy strength, and the tensile fracture path mainly within the stir nugget zone at aluminum alloy butt side. The formation mechanisms of the Ti/Al butt-welded interface structures were detailed according to the analyses of the characteristics at the butt interface. A high-quality Ti/Al FSW butt joint could be obtained when lower tool rotating speed and lower pin-offset value towards titanium alloy butt side were used.

Key words: dissimilar friction stir welding; intermetallic compounds; weld interface; microstructure; mechanical properties

Recognition model of arc welding penetration using ICA-BP neural network GAO Xiangdong[1], LIN Jun[1], XIAO Zhenlin[2], CHEN Xiaohui[2] (1. Guangdong Provincial Key Laboratory of Computer Integrated Manufacturing, School of Electromechanical Engineering, Guangdong University of Technology, Guangzhou 510006, China; 2. Guangzhou Panyu Gofront Dyeing & Finishing Machinery Manufacturer Ltd., Guangzhou 511400, China). pp 33-36

Abstract: A BP neural network model based on ICA (Imperialist Competitive Algorithm) is proposed to recognize the arc welding penetration status. The weights and thresholds of the neural network are initialized using ICA which has the features of uneasy accessibility to local extremum and fast search speed. Then the BP algorithm is used to train the neural network. By capturing the images of the molten pool in welding process, three features of a molten pool image are processed. The features includes the weld pool area, weld pool width and the distance between the weld pool centroid and the bottom. These features are as the inputs of neural network to create the mapping relationship between the three features of molten pool and the weld penetration status, and eventually a predicted model of penetration status is established. Welding experimental results show that the welding penetration status can be accurately recognized using the ICA-BP neural network.

Key words: penetration; recognition; ICA; BP neural network

Joining mechanisms of Mg-steel butt welded joints by cold metal transfer method CAO Rui[1], ZHU Haixia[1], WANG Qing[2], DONG Chuang[2], LIN Qiaoli[1], CHEN Jianhong[1] (1. State Key Laboratory of Advanced Processing and Recycling of Nonferrous Metal, Lanzhou University of Technology, Lanzhou 730050, China; 2. Key Laboratory of Materials Modification by Laser, Ion and Electron Beams, Ministry of Education, Dalian University of Technology, Dalian 116024, China). pp 37-40

Abstract: In this paper, Mg AZ31 sheet and galvanized steel sheet were butt welded and joined by cold metal transfer method with AZ61 Mg wire. Weld appearance, tensile properties and microstructure of Mg-steel butt joints at various welding parameters were investigated by changing wire feed speeds and groove angles. Results indicated that Mg-steel brazed-welded joints with good weld appearance and 4.02kN of tensile load can be achieved. And the brazed-welded joint is composed of welded joint at Mg side and brazed joint at steel side. The brazed joint is made of two parts, one is Mg-galvanized steel brazed joint which is located at the top of galvanized steel sheet, and the other is Mg-bare steel brazed joint which is located at the groove side. The Mg-galvanized steel joint brazed interface is composed of two reaction layers with -Mg + MgZn eutectic phase and Fe/Al reaction layer. The Mg-bare steel brazed interface at the groove side is composed of Fe/Al reaction layer, and Fe/Al phase is diffused and reacted by Al element of the Mg wire and Mg base metal.

Key words: magnesium AZ31; galvanized steel; cold metal transfer; brazed-welded

Vacuum diffusion bonding of surface textured stainless steel and aluminum LIU Hai, ZHANG Lixia, REN Wei, FENG Jicai (State Key Lab of Advanced Welding and Joining, Harbin